Rev.Adv.Mater.Sci. 16(2007) 1-9

PLASTIC DEFORMATION AND FRACTURE PROCESSES IN METALLIC AND CERAMIC NANOMATERIALS WITH BIMODAL STRUCTURES

I.A. Ovid'ko and A.G. Sheinerman

Institute for Problems of Mechanical Engineering, Russian Academy of Sciences,
Bolshoj 61, Vas. Ostrov, St. Petersburg 199178, Russia

Received: September 17, 2007

Abstract. We briefly review the experimental data and theoretical concepts concerning plastic deformation and fracture processes in nanomaterials with bimodal structures. Special attention is paid to the peculiarities of plastic deformation of these materials that result in the combination of a high flow stress and strain to failure. Also, we suggest a theoretical model that describes the generation of nanoscale cracks at the boundaries between the large grains and nanoscale matrix. In the framework of the model, cracks are generated in the stress field of interfacial disclination dipoles formed at the interfaces between large grains and the nanocrystalline matrix during plastic deformation of nanomaterials with bimodal grain size distributions. The model predicts that the generation of cracks at such disclination dipoles is energetically favorable in metallic and ceramic nanomaterials with bimodal structures in wide ranges of their structural parameters.

1. INTRODUCTION

Metallic and ceramic nanocrystalline materials – solids with grain size lower than 100 nanometers – are characterized by superior values of strength and/or hardness, which are required in many applications; see, e.g., reviews [1–9] and book [10]. At the same time, nanocrystalline materials commonly have very low ductility which limits their practical utility. The low ductility of nanocrystalline materials is primarily attributed to the suppression of lattice dislocation slip (serving as the dominant deformation mode in conventional coarse-grained polycrystals) in nanoscale grains. Indeed, with the suppression of lattice dislocation activity, brittle cracks easily grow in nanocrystalline materials. Besides, in spite of the action of specific deformation mechanisms in nanocrystalline materials, the absence of both lattice dislocation accumulation and associated strain hardening during plastic deformation often makes these materials unstable with respect to plastic strain instability followed by necking [1–10].

In recent years, however, several approaches have been suggested allowing one to reach both a high strength and a good tensile ductility of nanocrystalline materials (see the general discussion in Refs. [3–6, 10–12]). One of these approaches is related to the fabrication of metallic and ceramic nanomaterials consisting of (sub)micrometer-size grains embedded into a nanocrystalline or ultrafine-grained matrix [3, 4, 10–25] (Fig. 1). The chemical compositions of large grains and the nanocrystalline matrix can be either identical or different. Obviously, such nanomaterials have two peaks in grain size distribution, one in the nanometer range, and the other in the (sub)micrometer range. Therefore, these are referred to as nanomaterials with a bimodal grain size distribution or simply as nanomaterials with bimodal structures.

Corresponding author: I.A. Ovid'ko, e-mail: ovidko@def.ipme.ru

Although the physical processes acting in nanomaterials with bimodal structures in the course of their plastic deformation are not yet clear enough, the general assumption is that the presence of large grains suppresses crack growth and provides strain hardening (that stops plastic strain instabilities and catastrophic necking). Both these factors are necessary for good ductility, while the presence of the nanocrystalline matrix results in high strength and hardness of nanomaterials with bimodal structures. In this paper, we briefly review the experimental data and theoretical concepts concerning plastic deformation and fracture processes in nanomaterials with bimodal structures (section 2). Also, we suggest a theoretical model that describes the generation of nanoscale cracks at the boundaries between the large grains and nanocrystalline matrix (section 3). Section 4 contains concluding remarks.

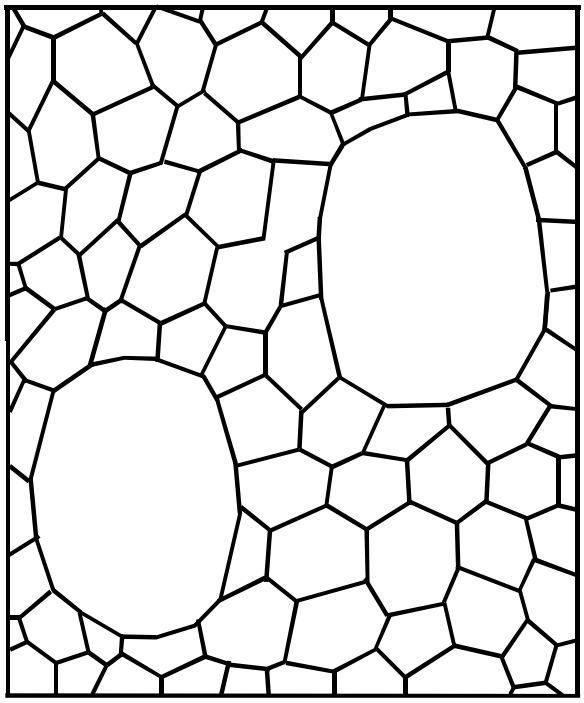

Fig. 1. Nanomaterial with a bimodal structure (schematically).

2. REVIEW ON THE PLASTIC DEFORMATION AND FRACTURE PROCESSES IN NANOMATERIALS WITH BIMODAL STRUCTURES

Apparently, the first experimental investigation of bimodal nanomaterials was performed by Tellcamp *et al.* [13], who fabricated a nanostructured aluminum alloy with an average grain size of 30 to 35 nm. The nanostructured alloy has been found to have a 30% increase in yield strength and ultimate strength compared to the strongest form of this alloy, with no corresponding decrease in elongation. The enhanced ductility has been attributed to the presence of a few large aluminum grains. It was supposed that dislocation activity in these grains could blunt the propagating cracks and thereby enhance plasticity.

More recently, Zimmerman *et al.* [14] have produced nanocomposite materials consisting of a nanocrystalline Ni matrix (with the grain size of 10–15 nm) reinforced with sub-micron size SiC particles (with the average particle size of 400 nm). The resulting nanocomposite materials with a bimodal grain size distribution demonstrated substantial improvements in hardness, yield and tensile strength, compared to conventional Ni–SiC composites with a matrix grain size in the micrometer range. The obtained materials have demonstrated tensile strengths up to four times as large as the strength of conventional polycrystalline Ni and two times as large as that of conventional polycrystalline Ni–SiC of comparable SiC content. The tensile and yield strengths of the nanocomposite material with SiC content less than 2 vol.% were higher than those for pure nanocrystalline Ni of comparable grain size. For these nanocomposites an increase in tensile ductility was also observed when compared to pure nanocrystalline nickel. At higher SiC content the strength and ductility were found to decrease. According to Zimmerman *et al.* [14], this may be associated with SiC particle clustering accompanied by the formation of pores between neighboring particles. The number of pores increases with the content of the SiC phase, thus weakening the nanocomposite.

Wang *et al.* [15] and Wang and Ma [12] fabricated *in situ* formed Cu with a bimodal grain size distribution. To do so, they used equal-channel angular pressing followed by cryo-rolling, i.e., cold rolling at a low temperature, and recrystallization at 200 ° C. The obtained bimodal structure showed both good ductility, with a high tensile strain to failure (about 65% in terms of engineering strain), and a high yield stress of more than 300 MPa, which is several times larger than the yield stress of coarse-grained Cu. In contrast to the case of nanocrystalline Cu specimens, which demonstrated deformation softening and associated plas-

tic strain instability directly after yielding, the Cu specimens with a bimodal structure demonstrated essential strain hardening, resulting in their good ductility. The postmortem transmission electron microscopy observations of the specimens with a bimodal structure have demonstrated the presence of dislocations in large (micrometer-size) grains. According to Wang and Ma [12], one of the factors responsible for strain hardening is the twinning deformation observed in the larger grains. Such a deformation mode is not expected at room temperature and quasi-static strain rates for pure Cu, which deforms at a relatively low stress level. At the same time, during the deformation of the inhomogeneous bimodal structure at high stress levels, the required high stress for twinning can be reached, at least, at the places of stress concentrations at the grain boundaries.

He *et al.* [16, 20] fabricated bimodal Ti-based alloys, which exhibits up to 14.5% compressive plastic strain at room temperature, with the yield stress of 1.2 GPa and ultimate compression stress of 2.4 GPa. They observed extensive shear banding in the nanocrystalline matrix of the plastically deformed bimodal Ti-based alloy. Some of the shear bands bypassed dendrites while others cut through them. This confirmed that the dendrites contribute to the plastic deformation by dislocations. However, dendrites retarded the catastrophic propagation of shear bands typical of plastically deformed nanocrystalline materials. Similarly, dendrites were observed to retard microcrack propagation. Microcracks bypassed some dendrites but then were stopped by other dendrites. Thus, He *et al.* [16, 20] clearly demonstrated the obstruction by dendrites on shear-banding and fracture. Similar results have been obtained by Das *et al.* [17, 18] for Zr-based composites consisting of dendrites in a nanocrystalline matrix.

Han *et al.* [24] fabricated bimodal 5083 Al alloys with nanograins of about 200 nm in size and large grains with the size of about 1 μm. Although the fabricated bimodal alloys have better ductility than ultrafine-grained alloys with the same composition, the fabricated alloy exhibited no strain hardening (and even strain softening in the tensile tests).

Fan *et al.* [25] produced bimodal Al-Mg alloys with ultrafine-grained Al matrix and micrometer-size large grains. The compressive tests showed strain to failure of 30-40%, depending on the strain rate. Scanning electron microscopy (SEM) observations at the compressive strain of 20% clearly demonstrated, besides the plastic deformation localized in large grains, the presence of a high density of shear bands propagating along about 45º to the direction of the applied load. The distance between the shear bands was approximately equal to the average grain size in the ultrafine-grained matrix. SEM observations also demonstrated that the sample fractures along a direction with a maximum shear force, i.e., approximately 45º to the loading direction. The tensile tests revealed tensile strain to failure of 8%, which is much larger than that for a homogeneous ultrafine-grained Al-Mg alloys (less than 1%). Shear bands were also observed on the surface during the tensile test. According to Fan *et al.* [25], relatively good ductility of bimodal Al-Mg alloys is associated with dislocation motion and multiple shear banding, in contrast to a single dominant shear band that often develops in monolithic ultrafine-grained Al-Mg alloys, leading to a very limited ductility of these alloys.

In the course of the tensile deformation of the bimodal Al-Mg alloy [25], cavitations were observed on the surface of the deformed sample, and were particularly concentrated close to the fracture area. The cavitations were attributed to the unaccommodated strain between coarse grains and ultrafine grains, since coarse grains may experience more plastic strain than ultrafine grains. Apparently, the formation of cavities can be a means to release high elastic stresses around dislocations accumulated at the interfaces between the large grains and ultrafine-grained matrix during plastic deformation. Tensile plastic deformation of bimodal Al-Mg alloys was also accompanied by necking, which had not been observed in the monolithic ultrafine-grained Al–Mg alloy of the same composition. Therefore, the combination of cavitation, necking, and shear localization is responsible for fracture of Al-Mg bimodal alloys during the tensile deformation.

Deformation of alloys with bimodal grain size distributions has also been analyzed numerically by Ye *et al.* [22] within a two-dimensional self-consistent embedded unit-cell model [26, 27] (see also review [4]). This model is based on the continuum mechanics description of a random array of particles in a composite material. The model was used to calculate the stress and strain distributions in uniaxially deformed bimodal nanostructured Al alloys [23, 24]. It has been observed that the stress and strain distributions remain uniform immediately after yielding. At the same time, as plastic deformation starts, the stress field becomes heterogeneous and the plastic strain tends to be concen-

trated in the vicinity of interphase boundaries at the faces of submicron grains.

Han *et al.* [23] also experimentally observed crack propagation in bimodal Al alloys. They have demonstrated that during tensile testing microcracks first formed in the nanograins. The cracks advanced perpendicular to the loading direction and then were stopped at the interfaces of the large grains and the nanocrystalline matrix. As plastic deformation proceeded, the interface between the coarse grains and nanograins delaminated and the coarse grains developed necking and eventually fractured.

The experimental observations summarized above testify that the processes of plastic deformation and fracture of nanomaterials with bimodal structures are influenced by the interfaces between the nanocrystalline matrix and large grains. First, dislocations that slip in large grains under the action of an applied stress can be stopped at these interfaces. Independent of whether these stay at the interfaces or propagate into the nanocrystalline matrix as the applied stress increases and deformation proceeds, the dislocations at the interfaces form groups and create interface steps. For geometric reasons, the formation of the interface steps is accompanied by the generation of disclination dipoles (rotational defects) [28]. These disclination dipoles create high local stresses whose relaxation can occur through the nucleation and propagation of cracks, which have been observed at the interfacial areas between the nanocrystalline matrix and large grains; see, e.g., [4]. The mechanism for the formation of disclination dipoles at the interfaces between large grains and the nanocrystalline matrix and the conditions for crack nucleation in the stress field of the disclination dipoles will be examined in the next sections.

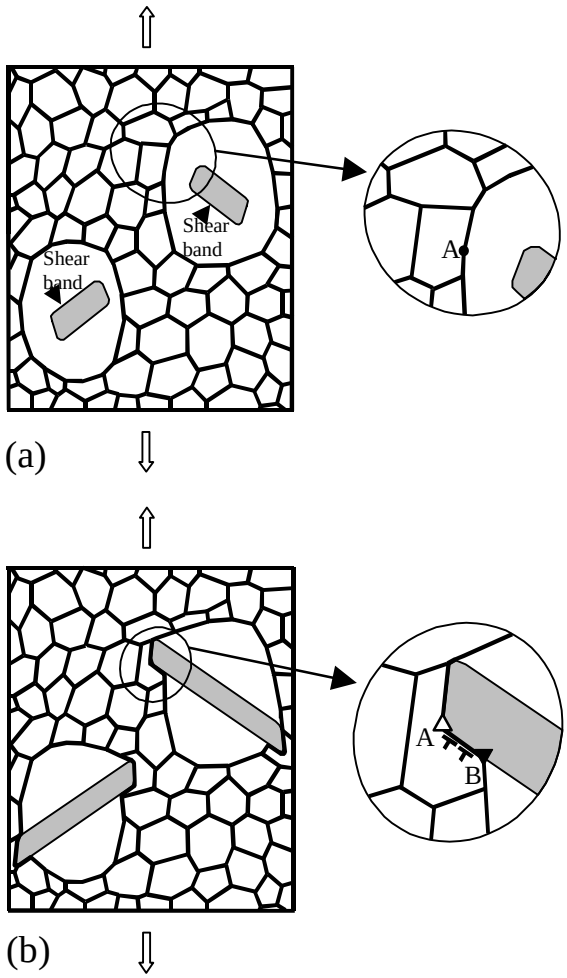

Fig. 2. Formation of disclination dipoles and dislocations in plastically deformed materials with a bimodal structure. (a) Shear bands are generated in large grains and propagate towards grain boundaries. (b) When shear bands reach grain boundaries, interface steps form that contain both a disclination dipole and dislocations. The large ellipses give the magnified view of the region surrounding one of the moving shear band edges.

3. FORMATION OF DISCLINATION DIPOLES AND NANOCRACK NUCLEATION AT INTERFACES IN DEFORMED NANOMATERIALS WITH A BIMODAL STRUCTURE

Plastic deformation in nanocrystalline solids is strongly influenced by interfaces. In particular, grain boundaries hamper intragrain slip carried by lattice dislocations. These hampering effects are, in part, related to the formation of disclination dipoles at the places of intragrain slip across grain boundaries. One of the basic ways for the formation of disclination dipoles at the interfaces between large grains and the nanocrystalline matrix in nanomaterials with a bimodal structure is as follows. Lattice dislocations move under the action of an applied stress within large grain interiors and often form either dislocation pile-ups or shear bands (Fig. 2a). When a dislocation pile-up or shear band reaches a grain boundary, an interface step forms which contains a disclination dipole (Fig. 2b). The formation of an interface step is accompanied by the transfer of a triple junction with the adjacent grain boundary (GB) from its initial position A to a

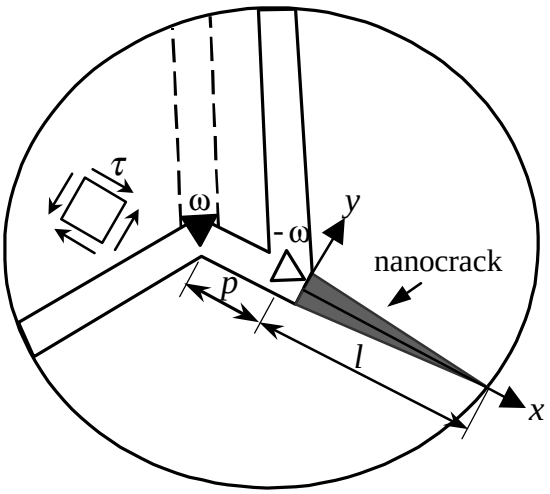

Fig. 3. Geometry of a nanocrack formed at a disclination dipole.

new position B. As a result of the transfer, the angle gaps ω and -ω appear at the GB junctions A and B, respectively, where ω is the tilt misorientation of the moving GB [28]. In the theory of defects in solids, the junctions A and B with the angle gaps ±ω represent wedge disclinations which are characterized by the strengths ±ω [29] and form a dipole configuration.

Thus, dislocation dipoles can form in deformed nanomaterials with a bimodal structure at the interfaces between the nanocrystalline matrix and large grains. The role of such dipoles in initiating cracks in their vicinity will be theoretically examined in the rest of this section.

Let us consider the model situation where a nanocrack nucleates in the stress field of a dipole of disclinations with the strengths ±ω formed due to GB sliding (Fig. 3). The nanocrack is assumed to have a length l and nucleate at the disclination with the strength -ω, along a GB in the region where the tensile stresses exerted on the crack surfaces by the disclination dipole are highest (see Fig. 3).

Let us introduce a coordinate system (x, y) as shown in Fig. 3. In this coordinate system the disclinations with the strengths ω and -ω lie at the x-axis at the points $x = -p$ and $x = 0$, respectively. To calculate the conditions for nanocrack growth, we will use the energetic criterion [30, 31]

$$F > 2\gamma_e, \tag{1}$$

where F is the energy release rate, $\gamma_e = \gamma - \gamma_b/2$, γ is the the specific surface energy, and γ_b is the GB energy per unit area. The term γ_b appears in formula (1) because GB cracks remove the GB fragment characterized by an excess specific energy.

To calculate the energy release rate F, we model the nanomaterial as an elastically isotropic solid with a shear modulus G and Poisson's ratio ν. In the considered case of an elastically isotropic solid and plane strain state, the energy release rate is calculated as [30]

$$F = \frac{\pi(1-\nu)l}{4G}\left(\overline{\sigma}_{yy}^2 + \overline{\sigma}_{xy}^2\right), \tag{2}$$

where $\overline{\sigma}_{yy}$ and $\overline{\sigma}_{xy}$ are the mean weighted values of the stresses $\overline{\sigma}_{yy}$ and $\overline{\sigma}_{xy}$, created by the applied stress τ and disclination dipole. The mean weighted stresses $\overline{\sigma}_{yy}$ and $\overline{\sigma}_{xy}$ are defined as [30]

$$\overline{\sigma}_{my} = \frac{2}{\pi l}\int_0^l \sigma_{my}(x, y=0)\sqrt{\frac{x}{l-x}}dx,\ m = x, y. \tag{3}$$

The stresses $\sigma_{xy}(x,y=0)$ and $\sigma_{yy}(x,y=0)$ are given by [29]: $\sigma_{xy}(x,y=0) = \tau$, $\sigma_{yy}(x,y=0) = D\omega\ln|(x+p)/x|$, where $D = G/[2\pi(1-\nu)]$. Substitution of the latter expressions for σ_{xy} and σ_{yy} and formulae (2) and (3) to (1) yields the following condition of energetically favorable nanocrack growth: $q(\tilde{l}) > q_c$, where $\tilde{l} = l/p$,

$$q(\tilde{l}) = \tilde{l}\left[\left(\frac{2\sqrt{1+\tilde{l}}-1}{\tilde{l}} - \ln\frac{\sqrt{1+\tilde{l}}+1}{\sqrt{1+\tilde{l}}-1}\right)^2 + \left(\frac{\tau}{D\omega}\right)^2\right], \tag{4}$$

and $q_c = 32\pi(1-\nu)\gamma_c/(Gp\omega^2)$.

With the above formulae, we calculated both q_c and the dependence $q(\tilde{l})$ (see Fig. 4) in the exemplary case of τ = 1 GPa, ω = π/6, $\gamma_b = 0.5\gamma$ and the following parameters of nanocrystalline α-Al_2O_3 (corundum) [32, 33]: G = 169 GPa, ν = 0.23, γ = 1.69 J/m^2. The solid and dashed lines show the values of q_c for p = 5 nm and 2 nm, respectively. As follows from Fig. 4, $q(\tilde{l})$ first increases and then decreases with rising $\tilde{l}$. Nanocrack nucleation and growth in the range $l < l_{e1}$ requires thermal fluctuations. Its subsequent growth within the length range $l_{e1} < l < l_{e2}$ occurs athermally. Further nanocrack growth is energetically forbidden.

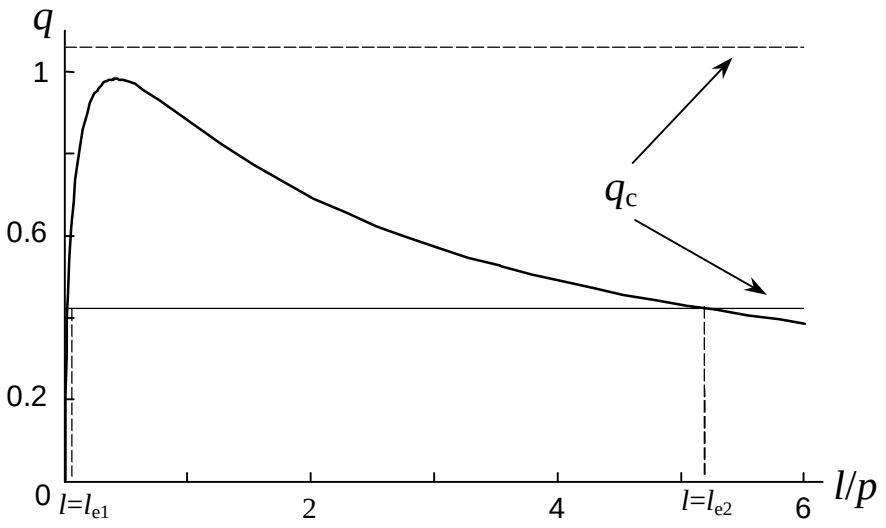

Fig. 4. Dependence of the parameter q on the normalized nanocrack length l/p for α-Al_2O_3. The solid and dashed horizontal lines show the values of the parameter q_c for p = 5 nm and p = 2 nm, respectively.

The dependences of the critical nanocrack lengths l_{e1} and l_{e2} on disclination strength ω and dipole arm p are shown in Fig. 5a and Fig. 5b, respectively, for the cases of α-Al_2O_3 and 3C-SiC. The dependences are shown for $\tau = 1$ GPa, $\gamma_b = \gamma/2$, p = 3 nm (a) and $\omega = \pi/4$ (b). As is seen in Fig. 5, for small enough ω and/or p, the critical lengths l_{e1} and l_{e2} do not exist. In this case, nanocrack growth is energetically unfavorable at any crack length, that is, the nanocrack does not form. From Fig. 5 it also follows that with an increase in ω and/or p, the nanocrack length interval (l_{e1}, l_{e2}) where nanocrack growth is energetically beneficial, expands. Notice that at large enough values of disclination strength ω the critical length l_{e1} is very small, whereas the equilibrium nanocrack length l_{e2} is comparable with the grain size of the nanocrystalline matrix. For example, for α-Al_2O_3 with $\gamma_b = \gamma/2$, $\omega = \pi/6$, p = 5 nm and d = 50 nm we have: $l_{e1} \approx 0.03p$ = 0.15 nm (that is, in fact, l_{e1} = 0), while $l_{e2} \approx 5p = d/2$. For 3C-SiC (with the following parameter values [34]: G = 217 GPa, ν = 0.23 and γ = 1.84 J/m^2) for $\gamma_b = \gamma/2$, $\omega = \pi/6$, p = 5 nm and d = 50 nm, we have: $l_{e1} \approx 0$, $l_{e2} \approx 6.5p = 0.65d$. In other words, in these cases the equilibrium nanocrack length l_{e2} is equal to the half of the grain size or even more.

As it has already been mentioned above, for high enough values of p and ω, the equilibrium length l_{e1} may be very small (less than the interatomic distance). In this case, the nanocrack can nucleate in a non-barrier way, without the need to overcome an energetic barrier using thermal fluctuations. Suppose that the non-barrier formation of a nanocrack is possible if the nanocrack length is smaller than some critical distance x_m from the disclination with the strength $-\omega$. The critical distance x_m is defined as the boundary of the region $x < x_m$, where the tensile stress σ_{yy} (see Fig. 3) created by the disclination dipole in the absence of the nanocrack exceeds the theoretical fracture strength. At $x = x_m$ this stress becomes equal to the theoretical fracture strength. As a first approximation, we assume the theoretical fracture strength to equal $G/(2\pi)$. Then in the coordinate system of Fig. 3, the condition of non-barrier formation of the nanocrack can be written as $l_{e1} < x_m$, where the length x_m follows from the equation $\sigma_{yy}(x_m, y = 0) = G/(2\pi)$. Substituting the relation $\sigma_{yy}(x_m, y = 0) = D\omega \ln|(x_m + p)/x_m|$ to this equation, we obtain the following expression for x_m:

$$x_m = \frac{p}{\exp\left[(1-\nu)/\omega\right] - 1}. \qquad (5)$$

From formula (5), the relation $x_m < l_{e1}$ and equation $q(l_{e1}/p) = q_c$ for the calculation of l_{e1}, at the specified values of the applied stress and materials parameters, we calculate the parameter regions (ω,

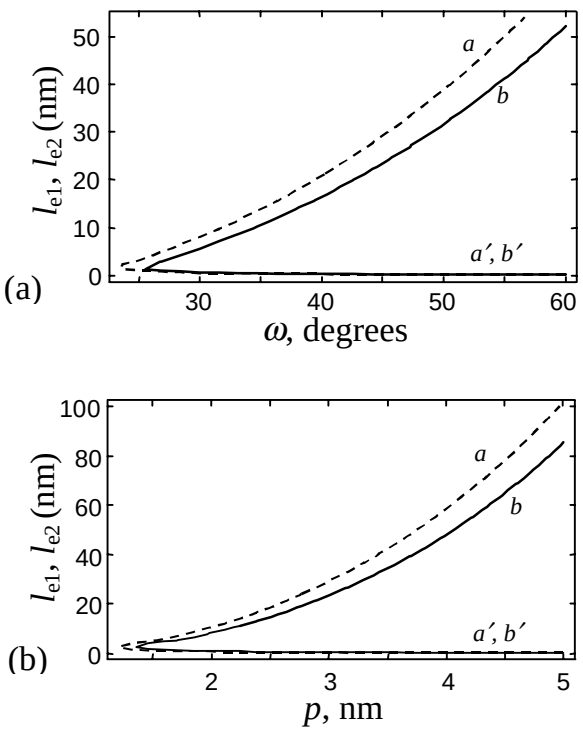

Fig. 5. Dependences of the critical nanocrack lengths l_{e1} (curves a' and b') and l_{e2} (curves a and b) on disclination strength ω (a) and dipole arm p (b) for 3C-SiC (curves a and a') and α-Al_2O_3 (curves b and b'). The dependences are drawn for τ =1 GPa, $\gamma_b = \gamma/2$, p = 3 nm (a) and ω = π/4 (b).

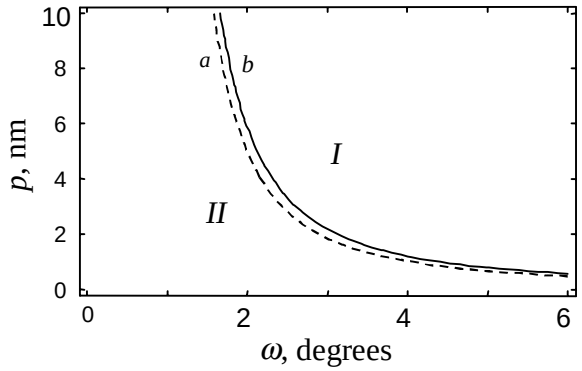

Fig. 6. Curves *a* and *b*, drawn for 3C-SiC and α-Al_2O_3, respectively, separate the parameter regions (ω, p), where nanocracks can nucleate in a non-barrier way (region *I* above the corresponding curve) from the parameter regions where nanocrack generation requires overcoming an energetic barrier (region *II* below the corresponding curve). The curves are drawn for τ = 1 GPa.

p) where the nanocrack can nucleate in a non-barrier way. These parameter regions in the coordinates (ω, p) are shown in Fig. 6 for the cases of 3C-SiC and α-Al_2O_3 at τ = 1 GPa. Curves *a* and *b* in Fig. 6, drawn for 3C-SiC and α-Al_2O_3, respectively, separate the parameter region (ω, p), where the nanocrack nucleates in a non-barrier way (above the corresponding curve) from the parameter region where nanocrack nucleation requires overcoming an energetic barrier (below the corresponding curve). As is seen in Fig. 6, at small p (< 2 nm), the possibility for non-barrier nanocrack formation is primarily determined by the value of the dipole arm p, while at large p (> 5 nm), this possibility depends mostly on the disclination strength ω. In general, from Fig. 6 it follows that the non-barrier formation of nanocracks is possible at the disclination dipoles originating due to the migration of high-angle GBs, in a wide range of the parameters (arm p and disclination strength ω) of these dipoles.

4. CONCLUDING REMARKS

Thus, we have briefly reviewed the studies of the processes of plastic deformation and fracture in nanomaterials with bimodal structures, consisting of micrograins and the nanocrystalline matrix. The results of the reviewed experimental works demonstrate that these materials exhibit the unique combination of a high flow stress with good plasticity. Commonly, such a combination is not achieved in nanocrystalline or fine-grained materials with unimodal grain size distributions. Good ductility is treated to be due to large grains suppressing crack growth and providing strain hardening (that stops plastic strain instabilities and catastrophic necking). At the same time, the presence of a nanocrystalline matrix is responsible for high strength and hardness of nanomaterials with bimodal structures.

Since plastic deformation starts to occur in large grains and nanocrystalline matrix at different levels of the yield stress, plastic flow is inhomogeneous in nanomaterials with bimodal structures. Elastic stresses occur at the boundaries between the large grains and nanocrystalline matrix, and these boundaries can serve as nuclei of fracture processes. In this paper, we have suggested a theo-

retical model describing the generation of nanoscale cracks at the boundaries between the large grains and nanocrystalline matrix. In the framework of the model, lattice dislocations that slip in large grains are stopped at the boundaries of these grains and nanocrystalline matrix. The resulting interface steps lead to the formation of disclination dipoles that can initiate the generation of nanocracks. In particular, for ceramic nanomaterials with bimodal structures (3C-SiC and α-Al_2O_3), the formation of nanocracks at disclination dipoles with the arm of several nanometers is possible if these dipoles form due to the step formation at high-angle GBs. For sufficiently high values of the misorientation angles of the stepped boundaries (equal in magnitude to the strength of the dipole disclinations) nanocracks can nucleate in a non-barrier way, without thermal fluctuations. The equilibrium length of the nanocracks formed at such GBs can be of the order of the average grain size in the nanocrystalline matrix. As a consequence, such nanocracks can coalesce, leading to the nucleation and propagation of microcracks.

ACKNOWLEDGEMENTS

The work was supported, in part, by the Office of US Naval Research (grant N00014-07-1-0295), the Russian Federal Agency of Science and Innovations (Contract 02.513.11.3190), the National Science Foundation under Grant CMMI #0700272, CRDF (grant # RUE2-2684-ST-05), and Russian Academy of Sciences Program "Structural Mechanics of Materials and Construction Elements".

References

[1] K.S. Kumar, H. Van Swygenhoven and S. Suresh // *Acta Mater.* **51** (2003) 5743.
[2] S.C. Tjong and H. Chen // *Mater. Sci. Eng.* R **45** (2004) 1.
[3] X. Zhang, H. Wang and C.C. Koch // *Rev. Adv. Mater. Sci.* **6** (2004) 53.
[4] B.Q. Han, E. Lavernia and F.A. Mohamed // *Rev. Adv. Mater. Sci.* **9** (2005) 1.
[5] I.A. Ovid'ko // *Rev. Adv. Mater. Sci.* **10** (2005) 89.
[6] I.A. Ovid'ko // *Int. Mater. Rev.* **50** (2005) 65.
[7] D. Wolf, V. Yamakov, S.R. Phillpot, A.K. Mukherjee and H. Gleiter // *Acta Mater.* **53** (2005) 1.
[8] M.A. Meyers, A. Mishra and D.J. Benson // *Progr. Mater. Sci.* **51** (2006) 427.
[9] M. Dao, L. Lu, R. J. Asaro, J. T. M. De Hosson and E. Ma // *Acta Mater.* **55** (2007) 4041.
[10] C.C. Koch, I.A. Ovid'ko, S. Seal and S. Veprek // Structural Nanocrystalline Materials: Fundamentals and Applications (Cambridge University Press, Cambridge, 2007).
[11] C.C. Koch // *Scr. Mater.* **49** (2003) 657.
[12] Y.M. Wang and E. Ma // *Acta Mater.* **52** (2004) 1699.
[13] V.L. Tellkamp, A. Melmed and E.J. Lavernia // *Metall. Mater. Trans.* A **32** (2001) 2335.
[14] A.F. Zimmerman, G. Palumbo, K.T. Aust and U. Erb // *Mater. Sci. Eng.* A **328** (2002) 137.
[15] Y. Wang, M. Chen, F. Zhou and E. Ma // *Nature* **419** (2002) 912.
[16] G. He, J. Eckert, W. Löser and L. Schultz // *Nature Mat.* **2** (2003) 33.
[17] J. Das, A. Güth, H.-J. Klauß, C. Mickel, W. Löser, J. Eckert, S.K. Roy and L. Schultz // *Scripta Mat.* **49** (2003) 1189.
[18] J. Das, W. Löser, U. Kühn, J. Eckert, S.K. Roy and L. Schultz // *Appl. Phys. Lett.* **82** (2003) 4690.
[19] E. Ma // *Nature Mater.* **2** (2003) 7.
[20] G. He, M. Hagiwara, J. Eckert and W. Löser // *Phil. Mag. Lett.* **84** (2004) 365.
[21] A.V. Sergueeva, N.A. Mara and A.K. Mukherjee // *Rev. Adv. Mater. Sci.* **7** (2004) 67.
[22] R.Q. Ye, B.Q. Han and E.J. Lavernia // *Metall. Mater. Trans.* A **36** (2005) 1833.
[23] B.Q. Han, Z. Lee, D. Witkin, S.R. Nutt and E.J. Lavernia // *Metall. Mater. Trans.* A **36** (2005) 957.
[24] B.Q. Han, J.Y. Huang, Y.T. Zhu and E.J. Lavernia // *Acta Mater.* **54** (2006) 3015.
[25] G.J. Fan, H. Choo, P.K. Liaw and E.J. Lavernia // *Acta Mater.* **54** (2006) 1759.
[26] E.V.D. Giessen and A. Needleman // *Annu. Rev. Mater. Res.* **32** (2002) 141.
[27] S. Schmauder // *Annu. Rev. Mater. Res.* **32** (2002) 437.
[28] I.A. Ovid'ko and A.G. Sheinerman // *Appl. Phys. Lett.* **90** (2007) 171927.
[29] A.E. Romanov and V.I. Vladimirov, in *Dislocations in Solids*, edited by F. R. N. Nabarro (North-Holland, Amsterdam, 1992), Vol. 9, p. 191.
[30] V.L. Indenbom // *Sov. Phys. Solid State* **3** (1961) 1506.

[31] I.A. Ovid'ko and A.G. Sheinerman // *Acta Mater.* **52** (2004) 1201; **53** (2005) 1347.
[32] R.G. Munro // *J. Amer. Cer. Soc.* **80** (1997) 1919.
[33] Z. Lodziana and J.K. Norskov // *J. Chem. Phys.* **115** (2001) 11261.
[34] Z. Ding, S. Zhou and Y. Zhao. *Phys. Rev.* B **70** (2004) 184117.